Spiking QRS Detector: Adaptive Homeostatic Modulation for Continual Unsupervised Learning

Kaveh Samiee

Abstract

A biologically plausible, shallow spiking neural network (SNN) is proposed for online QRS detection in single-channel electrocardiogram (ECG) signals, implementable on neuromorphic devices. The proposed method incorporates continuous adaptation to the spatiotemporal dynamics of QRS morphology. At each time step T, the preceding two-second chunk of the amplitude-squared streaming ECG signal is encoded using a Poisson rate coding scheme of length N . Subsequently, these spike trains are fed to a two-layer SNN sample by sample. After each forward pass, the spike-timing-dependent plasticity (STDP) learning rule, augmented with a novel adaptive homeostatic synaptic plasticity and excitability modulation mechanism, is applied to update inter-layer connection weights. The self-regulating learning mechanism involves adjusting the weights and membrane potential thresholds of the neurons based on the timing of spikes and their firing rate deviations to stabilize the network activity in accordance with the QRS complexes in each ECG segment. R-peak localization is achieved by detecting local maxima of the amplitude-squared signal during periods of burst spiking activity. Comparative analysis against state-of-the-art QRS detection algorithms indicates the superiority of the proposed method and its robustness for real-time implementation.

1. Introduction

Electrocardiogram (ECG) analysis is the most commonly used tool for the detection and diagnosis of cardiovascular diseases. Among ECG wave complexes, the QRS complex is one of the most critical components for identifying cardiac abnormalities. Thus, detection and localization of QRS complexes is the key step for further delineation of ECG wave complexes.

Spiking neural networks (SNNs) provide a pivotal alternative due to their event-driven processing and their biological plausibility. SNNs can efficiently process time-series signals, such as ECG, while maintaining low computational overhead. This paper proposes a biologically plausible shallow SNN for real-time detection of QRS complexes in single-channel ECG signal streams and as an alternative to traditional QRS detection methods. The proposed architecture incorporates continuous adaptation to the spatiotemporal dynamics of QRS morphology and amplitude, leveraging spike-timing-dependent plasticity (STDP) and homeostatic synaptic plasticity. Homeostatic plasticity is critical for regulating neuronal firing thresholds, ensuring that the network maintains balanced activity levels. In addition, to ensure that the SNN adapts to variations in both the timing and amplitude of QRS complexes, a self-regularization term is incorporated into the homeostatic mechanism, enhancing detection accuracy in dynamic ECG signal streams.

2. STDP with Homeostatic Synaptic Plasticity

Let us consider $U_i(t)$ to represent the membrane potential of the neuron labeled i at a particular discrete time point t. The behavior over time of $U_i(t)$ is characterized by the leaky integrate-and-fire (LIF) model, which can be mathematically described by the following equation:

$$U_i(t+1) = U_i(t) + \frac{\Delta t}{\tau_m}\left(-\big(U_i(t) - U_{\text{rest}}\big) + I_i(t)\right), \quad (1)$$

where τ_m denotes the time constant associated with the neuron's membrane, U_{rest} represents the neuron's potential during a resting state, $I_i(t)$ corresponds to the current input received by neuron i at the particular time t, Δt indicates the discrete interval of time between successive observations. The LIF neuron spikes when the membrane potential exceeds a threshold U_{th}:

$$\Theta_i(t) = \begin{cases} 1, & \text{if } U_i(t) \geq U_{\text{th}}, \\ 0, & \text{otherwise.} \end{cases} \quad (2)$$

After spiking, the neuron is reset to a potential U_{reset}. The spike output of the layer j is recorded over T time steps in the spike train matrix:

$$\mathbf{S_j} = \begin{bmatrix} \Theta_{1j}(1) & \Theta_{1j}(2) & \dots & \Theta_{1j}(T) \\ \Theta_{2j}(1) & \Theta_{2j}(2) & \dots & \Theta_{2j}(T) \\ \vdots & \vdots & \ddots & \vdots \\ \Theta_{Nj}(1) & \Theta_{Nj}(2) & \dots & \Theta_{Nj}(T) \end{bmatrix}, \quad (3)$$

where $\Theta_{ij}(t)$ represents the Heaviside step function for neuron i at time t, and N is the number of neurons in the layer j. Spike-timing-dependent plasticity (STDP) is a well-established biological learning rule observed in spiking neurons. There are several variations of STDP, but the core idea is that synaptic weights are updated depending on the precise timing of presynaptic and postsynaptic spikes. The most common form of STDP is expressed as:

$$\Delta w = \begin{cases} A_+ e^{-\Delta t/\tau_+} & \text{if } \Delta t > 0 \text{ (LTP)} \\ -A_- e^{\Delta t/\tau_-} & \text{if } \Delta t < 0 \text{ (LTD)} \end{cases} \tag{4}$$

where A_+ and A_- are the learning rates for long-term potentiation (LTP) and long-term depression (LTD), respectively, which control the strength of weight changes. τ_+ and τ_- are time constants that describe the temporal window over which potentiation and depression decay. $\Delta t = t_{\text{post}} - t_{\text{pre}}$ is the time difference between the postsynaptic spike (t_{post}) and the presynaptic spike (t_{pre}). This formulation is consistent with standard literature such as Hebb's rule and STDP in spiking neural networks [1].

STDP is closely related to Hebbian learning, which can be considered a special case of STDP. Hebb's rule, often summarized as "cells that fire together, wire together," describes how synaptic weights are strengthened if pre- and postsynaptic neurons fire in close succession. Hebbian learning is based on the correlation between the activity of two neurons, and it provides the foundational principle for many biologically plausible learning rules. In the case of STDP, the correlation is refined further by taking into account the exact timing difference between the spikes of the pre- and postsynaptic neurons, providing a more dynamic and precise learning rule for synaptic modification [2].

In physiology and neuroscience, homeostasis refers to the ability of an organism to maintain stability by making transient adaptations to external stimuli and environment changes [3]. Analogously, in bio-inspired neural network such as the spiking neural network, homeostasis is defined as the network ability to self-regulate the overall activity level of neurons, preventing neurons from becoming excessively excitable or entirely inactive. This is commonly achieved by adjusting synaptic plasticity of neurons according to input changes to maintain a stable firing rate over time. Homeostatic synaptic plasticity rule has been adapted from homeostatic plasticity models such as the Bienenstock-Cooper-Munro (BCM) theory and Oja's Rule [4, 5], and is given by:

$$\Delta w_j = \eta(\theta - r_j)w_j, \tag{5}$$

where Δw_j is the change in synaptic weights for the j-th layer, η is the learning rate, θ is the target firing rate of the layer (the homeostatic set-point), w_j is the current synaptic weight, and r_j is the average firing rate of the postsynaptic neurons in the layer j over time, defined as:

$$r_j = \frac{1}{NT}\|\mathbf{S_j}\|_\mathbf{1}, \tag{6}$$

where r_j is the firing rate of neurons at layer j, T is the number of time steps, N is number of neurons, and $\|\mathbf{S_j}\|_\mathbf{1}$ is ℓ_1-norm of $\mathbf{S_j}$.

This rule ensures that if a neuron's firing rate exceeds its target θ, synaptic weights are decreased to reduce excitability, whereas if the firing rate is below the target, synaptic weights are increased to enhance responsiveness.

Homeostatic plasticity and STDP operate in complementary manner. While STDP adjusts synaptic weights based on based on spike-timing relationships, homeostatic plasticity helps to maintain the overall stability of spiking neural networks by regulating the firing rate of neurons. In essence, homeostatic mechanisms counter-balances STDP-driven modifications in synaptic weights[4]. This interplay is crucial to ensure that neurons are able to learn and adapt while maintaining stable activity levels. STDP and homeostatic plasticity can be combined as follows:

$$\Delta w_j = \eta(\theta - r_j)w_j + \begin{cases} A_+ e^{-\Delta t/\tau_+} & \text{if } \Delta t > 0 \text{ (LTP)} \\ -A_- e^{\Delta t/\tau_-} & \text{if } \Delta t < 0 \text{ (LTD)} \end{cases}. \tag{7}$$

3. Homeostatic Membrane Potential Threshold Modulation

Some ion channels in biological neurons, such as the h-channel, regulate neuronal excitability by adjusting the resting membrane potential in response to prolonged activity [6]. Inspired by this biological mechanism, we propose a homeostatic membrane potential threshold modulation is proposed to dynamically adjust the firing thresholds of the neurons in response to their firing rates, ensuring that the neurons maintain stable activity levels over time. Based on the calculated firing rate, the output layer's threshold is adjusted as follows:

$$\Delta U_{\text{th},j} = \begin{cases} -\eta_j \times (\theta_{j,\min} - r_j) & \text{if } r_j < \theta_{j,\min}, \\ \eta_j \times 2 \times (r_j - \theta_{j,\max}) & \text{if } r_j > \theta_{j,\max}, \end{cases} \tag{8}$$

where η_j is the homeostatic learning rate, and $\theta_{j,\min}$ and $\theta_{j,\max}$ are the minimum and maximum target firing rates for the neuron. After adjusting the threshold, a decay factor is applied to allow the threshold to gradually return to an initial threshold value over time:

$$U_{\text{th},j} = \alpha\left(U_{\text{th},j} + \Delta U_{\text{th},j}\right) + (1-\alpha)U_{\text{th},j}^{\text{initial}}, \tag{9}$$

$$U_{\text{th},j} = \min\left(\theta_{j,\max}, \max\left(\theta_{j,\min}, U_{\text{th},j}\right)\right), \tag{10}$$

where $U_{\text{th},j}^{\text{initial}}$ refers to the initial threshold value before any stimuli.

4. Datasets and Experiments

To evaluate the performance of the proposed beat detection method, we use six publicly available datasets from PhysioNet. Namely, MIT-BIH Arrhythmia Database (MITBIH), QT Database (QTDB), MIT-BIH Supraventricular Arrhythmia Database (SVDB), T-Wave Alternans Database (TWADB), MIT-BIH Normal Sinus Rhythm Database (NSRDB), and MIT-BIH Noise Stress Test Database (NSTDB). These datasets provide a diverse range of ECG recordings, including both normal and abnormal cardiac rhythms. The total combined duration of all recordings is approximately 422 hours, containing over 2.2 million annotated heartbeats. A summary of beat counts per dataset is provided in Table 1. To mimic a wearable clinical scenario, only Lead II signals are used for beat detection across all datasets. Prior to conversion of ECG signal to spikes trains, the streaming ECG signals are first band-pass filtered within the frequency range of 8–22 Hz to isolate the QRS complex and suppress baseline wander and high-frequency noise. At each time step $T = 1$ second, the preceding two-second window of the amplitude-squared ECG signal is taken and encoded using a Poisson rate coding scheme of length $L = 10$. This encoding transforms the continuous signal into a set of spike trains. These spike trains are then fed into a two-layer SNN, with 10 and 5 neurons in first and second layers, sample-by-sample for real-time inference and beat detection.

4.1. Burst Detection in Spike Raster

During QRS complexes, the overall net deflection of ECG signal and subsequently pre-synaptic membrane potential of neurons in the first layer of a SNN are increased. The homeostatic membrane potential threshold modulation and the homeostatic plasticity mechanisms, ensure that this increased potential is populated to all pre/post synaptic neurons in all layers, exhibited as a spiking burst over the SNN network. To identify periods of burst spiking activity for each layer j over T, we employ a robust thresholding algorithm based on Gaussian smoothing and the median absolute deviation (MAD). Given a spike raster matrix $\mathbf{S_j} \in \{\mathbf{0}, \mathbf{1}\}^{\mathbf{N}\times\mathbf{T}}$ for layer j, we calculate the smoothed spike count as a function of time as follows:

$$\tilde{s}_j(t) = (s_j * G_\sigma)(t), \tag{11}$$

where $s_j(t) = \sum_{i=1}^{N} S_{j,i,t}$ represents the total spike count at time t across all N neurons in layer j, and $G_\sigma(\tau)$ is the Gaussian kernel with a standard deviation σ. The threshold cutoff for detecting burst regions is then derived as:

$$\tau_{\text{burst},j} = \text{median}(\tilde{s}_j) + \kappa \cdot \text{MAD}(\tilde{s}_j), \tag{12}$$

where κ is a tunable sensitivity parameter, and $\text{MAD}(\tilde{s}_j)$ is the MAD of the smoothed spike count. Burst spiking points can then be detected as:

$$B_j = \{t \mid \tilde{s}_j(t) > \tau_{\text{burst},j}\}. \tag{13}$$

Finally, contiguous intervals from B_j are selected by grouping consecutive time steps $t \in B_j$ into continuous segments $[t_{\text{start}}, t_{\text{end}}]$.

4.2. R-peaks localization

To reduce false positives (FP) caused by non-cardiac or non-QRS-related spike bursts, a chain of pruning rules is applied to prune spike burst regions based on their spiking activity. Each burst region is characterized by a set of temporal and structural features: burst duration, neuron participation, inter-spike interval coefficient of variation (ISI CV), and mean inter-spike interval (mean ISI). Bursts that deviate significantly from the statistical distribution of features extracted for all identified burst over T time steps are discarded. A burst is considered a false positive under the following conditions: 1) the burst duration is less than 300 milliseconds, 2) the burst duration is less than one quarter of the average duration of all bursts within the given time interval T, 3) the time distance from the last R-peak candidate is less then 250 milliseconds, 4) the burst duration and neuron participation of the current burst is smaller than those of the previous R-peak burst, 5) the ISI CV of the current burst is less than 1, and the mean ISI of the current burst is greater than that of the previous burst. R-peak localization is then achieved by detecting local maxima of the amplitude-squared signal within the pruned burst spiking regions.

Figure 1 illustrates a representative ECG segment from QTDB with detected R-peaks and corresponding spiking activity patterns. Table 1 summarizes the comparison of the proposed method's beat detection performance against several state-of-the-art methods in terms of true positive rate (TPR), positive predictive value (PPV), detection error rate (DER). The results demonstrate that the proposed spiking QRS detector achieves superior or competitive performance across all datasets, with the lowest detection error rates on MITBIH (0.77%) and QTDB (0.29%). Spiking QRS detector shows notable improvements in detection accuracy for challenging scenarios such as noisy environments (NSTDB), and significantly outperforms conventional algorithms in long-term monitoring scenarios (NSRDB), where it obtained the highest TPR (96.74%) and PPV (99.92%).

5. Conclusions

This study presents a novel biologically plausible SNN for real-time QRS detection, integrating STDP with adaptive homeostatic mechanisms. The shallow, event-driven

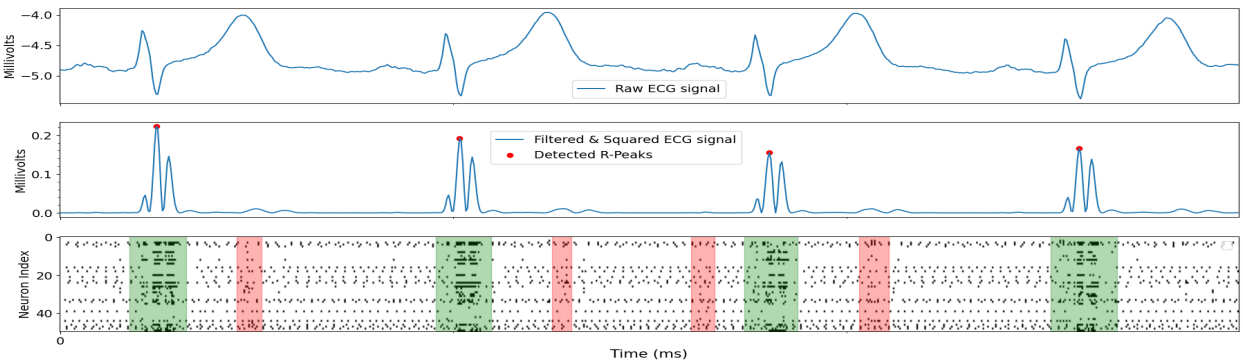

Figure 1: A three-second segment from record sele0604 of QTDB. Top: raw ECG signal. Middle: band-pass filtered/amplitude-squared signal and detected R-peaks. Bottom: corresponding spike raster plot and burst regions, discarded ones are highlighted in read.

architecture offers computational efficiency advantages for neuromorphic wearable devices while enabling unsupervised, privacy-preserving adaptation without patient-specific training. Future work should investigate multi-lead configurations, neuromorphic hardware implementation, and clinical validation.

6. Code Availability

The source code for this work is available at `https://github.com/KavehSam/SpikingQrs`

Table 1: Beat detection performance across different datasets

Dataset	# of Beats	Method	TPR%	PPV%	DER%
MITBIH	109,966	Spiking QRS	**99.53**	**99.72**	**0.77**
		Pan & Tompkins [7]	99.24	99.11	1.48
		Hamilton et al. [8]	97.98	98.68	3.18
		Elgendi et al. [9]	98.36	97.18	4.35
		Kalidas et al. [10]	97.25	99.15	3.71
QTDB	87,110	Spiking QRS	**99.76**	99.92	**0.29**
		Pan & Tompkins [7]	99.44	99.24	1.09
		Hamilton et al. [8]	99.61	99.46	0.81
		Elgendi et al. [9]	99.53	97.35	2.92
		Kalidas et al. [10]	99.32	**99.94**	0.78
SVDB	184,582	Spiking QRS	99.72	99.74	0.66
		Pan & Tompkins [7]	**99.84**	99.61	**0.65**
		Hamilton et al. [8]	99.39	**99.84**	0.85
		Elgendi et al. [9]	98.99	98.20	2.82
		Kalidas et al. [10]	99.15	99.74	1.08
TWADB	18,993	Spiking QRS	97.43	**98.03**	**4.66**
		Pan & Tompkins [7]	**98.09**	97.42	4.74
		Hamilton et al. [8]	97.58	94.69	7.88
		Elgendi et al. [9]	95.03	95.33	11.34
		Kalidas et al. [10]	95.85	96.44	7.79
NSRDB	1,799,697	Spiking QRS	**96.74**	**99.92**	**3.57**
		Pan & Tompkins [7]	92.69	99.71	7.42
		Hamilton et al. [8]	96.61	99.91	3.70
		Elgendi et al. [9]	96.76	84.82	20.84
		Kalidas et al. [10]	92.67	99.74	7.43
NSTDB	25,590	Spiking QRS	**96.13**	86.95	19.42
		Pan & Tompkins [7]	93.11	86.20	22.54
		Hamilton et al. [8]	94.63	87.11	20.28
		Elgendi et al. [9]	93.79	86.12	21.95
		Kalidas et al. [10]	93.59	**91.37**	**15.46**

References

[1] Fellous J, et al. Synaptic learning rules and the induction of spiking activity in neural networks. Computational neuroscience A comprehensive approach 2004;.

[2] Hebb DO. The Organization of Behavior: A Neuropsychological Theory. New York: John Wiley & Sons, 1949.

[3] Davies KJ. Adaptive homeostasis. Molecular aspects of medicine 2016;49:1–7.

[4] Turrigiano G. The self-tuning brain: Synaptic scaling of excitatory synapses. Cell 2008;135(3):422–435.

[5] Oja E. A simplified neuron model as a principal component analyzer. Journal of Mathematical Biology 1982; 15(3):267–273.

[6] Narayanan R, Johnston D. The h-channel: a key player in the regulation of neuronal excitability. Trends in Neurosciences 2010;33(5):288–295.

[7] Pan J, Tompkins WJ. A real-time qrs detection algorithm. IEEE Transactions on Biomedical Engineering 1985;BME-32(3):230–236.

[8] Hamilton P, et al. Beat detection in ecg signals: A computational approach. Journal of Electrocardiology 2002; 35(2):123–130.

[9] Elgendi M, Eskofier B, Dokos S, Abbott D. Revisiting qrs detection methodologies for portable, wearable, battery-operated, and wireless ecg systems. PLOS ONE 2014; 9(1):e84018.

[10] Kalidas V, Tamil LS. Real-time qrs detector using stationary wavelet transform for automated ecg analysis. In 2017 IEEE 17th International Conference on Bioinformatics and Bioengineering (BIBE). IEEE, 2017; 457–461.

Address for correspondence:

Kaveh Samiee

Pursimiehenkatu 26 C, 00150 Helsinki, Finland.

kaveh@doublepoint.com